Environmental Science: Atmospheres

ROYAL SOCIETY OF CHEMISTRY

PAPER

View Article Online
View Journal | View Issue

Cite this: *Environ. Sci.: Atmos.*, 2026, **6**, 76

Revealing discrepancies in potential driving factors of particulate-bound mercury between urban and suburban sites in a Southeast Asian megacity using a generalized additive model

Ly Sy Phu Nguyen, *[ab] Duc Thanh Nguyen,[ab] Le Quoc Hau,[ab] Guey-Rong Sheu*[c] and To Thi Hien[ab]

Particulate-bound mercury (PBM) plays a critical role in atmospheric mercury (Hg) cycling, yet its complex spatiotemporal variability and potential driving factors remain insufficiently understood, particularly in the Southeast Asia (SEA) region. This study reported year-round (May 2022 to April 2023) data of PBM at an urban (Nguyen Van Cu: 59.81 ± 29.15 pg m^{-3}) and a suburban site (Can Gio: 26.4 ± 9.59 pg m^{-3}) in southern Vietnam. Distinct seasonal trends were observed at both sites, with elevated PBM concentrations in the dry season (November–February), likely driven by changes in the source origin and transport paths of air masses. Lower PBM concentrations in the wet season (July–September) may result from enhanced removal by wet deposition, whereas limited rainfall in the dry season reduces this effect, leading to higher concentrations. We employed Generalized Additive Models (GAMs), which effectively captured nonlinear relationships between PBM and meteorological-chemical covariates. GAMs explained 87.7% of PBM variance in the urban area and 41.6% in the suburban area, indicating better model performance in urban *vs.* suburban areas. In the urban area, metals (*i.e.* Cr, Sr, Pb, and V) were the dominant contributors (36.7%), suggesting influence from industrial and traffic-related sources. In contrast, PBM at the suburban site was mainly modulated by temperature (60.8%), Zn (21.3%), and planetary boundary layer height (17.9%), pointing to the significance of atmospheric processes over local emissions. Our findings highlight the utility of GAMs in resolving complex PBM-environment interactions and indicate their potential for advancing source attribution and informing targeted mercury mitigation strategies.

Received 13th August 2025
Accepted 24th October 2025

DOI: 10.1039/d5ea00094g

rsc.li/esatmospheres

Environmental significance

Particulate-bound mercury (PBM) is a highly toxic form of atmospheric mercury, capable of regional-scale transport through complex atmospheric processes, posing substantial risks to ecosystems and public health. However, its behavior in tropical urban–suburban settings remains poorly characterized. This study provides the first year-round observational dataset of PBM in southern Vietnam, revealing distinct seasonal patterns and site-specific drivers. By employing generalized additive models, we indicated the effectiveness of data-driven approaches in disentangling complex PBM-environment relationships. Our findings suggest the contrasting roles of anthropogenic emissions and meteorological processes in shaping PBM levels in urban and suburban areas. These insights are essential for improving source attribution, supporting air quality management, and informing mercury mitigation strategies in rapidly developing regions of Southeast Asia.

1 Introduction

Mercury (Hg) is a persistent heavy metal with high bioaccumulation potential and has been shown to have significant adverse effects on human health and ecosystems.[1–3] Although it comprises less than 5% of total atmospheric Hg, particulate-bound mercury (PBM) plays a pivotal role in environmental processes owing to its relatively high deposition velocity and its function as a crucial vector connecting the atmosphere with other environmental compartments.[1,4] PBM originates from a mix of anthropogenic and natural sources and shows large differences in source contributions between different regions (*e.g.*, urban *vs.* suburban).[5,6] Key anthropogenic sources of PBM include combustion processes (*e.g.*, coal combustion), metal production, and various industrial activities, while natural sources involve volcanic eruptions and natural biomass burning.[6–9] These emissions are further influenced by atmospheric processes such as oxidation, adsorption, and condensation.[10–12]

[a]Faculty of Environment, University of Science, Ho Chi Minh City, Vietnam. E-mail: nlsphu@hcmus.edu.vn
[b]Vietnam National University, Ho Chi Minh City, Vietnam
[c]National Central University, Taiwan. E-mail: grsheu@atm.ncu.edu.tw

East and Southeast Asia (SEA) contribute approximately 38.7% of global anthropogenic Hg emissions, driven by rapid industrialization and urbanization.[2,13] Studies indicated the critical role of the East and SEA regions in the global Hg cycle.[6,13,14] While research in East Asia has advanced understanding of PBM sources and transport, significant uncertainties remain, particularly regarding PBM variability in the SEA region.[6,15–17] This shortage is mainly due to limited PBM data in SEA and the diverse emission sources, complex atmospheric chemistry, and region-specific meteorological conditions.[18] Improved characterization of PBM behavior in SEA is essential for identifying dominant sources and informing effective regional mitigation policies.

Source apportionment of PBM has traditionally relied on multivariate techniques such as Principal Component Analysis (PCA) and Positive Matrix Factorization (PMF).[18–21] While PCA reduces data dimensionality, it assumes linearity and permits negative loadings, limiting its interpretability.[22] PMF addresses non-negativity but still assumes linearity, requires pre-specifying the number of sources, and is sensitive to outliers.[20,23,24] To address the nonlinear relationships inherent in environmental data, Generalized Additive Models (GAMs) have been increasingly applied in air pollution research, including atmospheric Hg.[25–28] GAMs offer a flexible statistical framework that can model complex, nonlinear relationships between pollutant concentrations and environmental/meteorological variables without requiring prior assumptions about the functional form of these relationships.[25,26] For atmospheric Hg, Wu *et al.*[27] applied a GAM to quantify the contribution factors on TGM concentrations in Beijing, attributing 47.1% of the observed TGM variability to meteorological drivers. In a subsequent study, Wu *et al.*[28] employed a GAM to illustrate the effects of COVID-19 lockdown measures from meteorological influences such as relative humidity and temperature on TGM. These studies indicated the flexibility of GAMs in environmental modeling for capturing nonlinear environmental responses. However, the use of GAMs for PBM remains limited in the SEA region as well as in the literature. This represents a critical gap in the current understanding of PBM dynamics and their interactions with environmental factors.

In this study, we present a year-round observational dataset (May 2022–April 2023) on PBM concentrations and the elements of total suspended particles (TSP) obtained from two selected monitoring sites (urban and suburban) in Ho Chi Minh City (HCMC), Vietnam. From the perspective of particle size, TSP refers to the total fraction of airborne particles collected by a sampler without a size-selective inlet, typically capturing particles with aerodynamic diameters up to ~100 μm.[29] Unlike $PM_{2.5}$ or PM_{10}, TSP therefore encompasses both coarse and fine particles without a specific cutoff limit. HCMC is a representative megacity of Southeast Asia, characterized by rapid urbanization, high population density, and complex emission profiles. For the first time in this region, these data are integrated into a GAM model to explore key atmospheric processes influencing PBM. The primary aims of our study are: (1) to characterize the spatiotemporal variations in PBM concentrations across contrasting environments; (2) to investigate the relationships between PBM, chemical constituents of TSP, and meteorological parameters; and (3) to apportion and quantify the relative contributions of various anthropogenic and natural emission sources to PBM levels at both sites. The results from this study will not only enhance the understanding of PBM dynamics in SEA but also offer valuable insights for the development of targeted Hg mitigation strategies in rapidly growing urban centers across the region.

2 Materials and methods

2.1. Site description and TSP sampling

In this study, TSP samples were collected from two sites in HCMC (Fig. S1), representing contrasting environmental contexts: an urban site (Nguyen Van Cu – NVC; 10.762°N, 106.680°E) and a suburban/coastal site (Can Gio – CG; 10.402° N, 106.947°E). At the NVC site, TSP sampling was conducted on the rooftop of an 11-story building at the University of Science, VNU-HCM. The site is situated approximately 10 meters from a major multi-lane roadway and is influenced by anthropogenic emissions, particularly from vehicular traffic.[30] In contrast, the CG site is positioned on the second floor of Can Thanh High School in Can Gio District, approximately 50 km southeast of central HCMC. This site is located in a low-density residential area, about 40 meters from a local road and 400 meters inland from the coastline and is surrounded by extensive mangrove forests (Fig. S1). It is relatively isolated from major anthropogenic emission sources.[31,32] These monitoring sites have been applied in numerous atmospheric studies[18,32,33] and are considered representative of urban and suburban/coastal atmospheric environments in HCMC.

At the two monitoring sites, a total of 8 TSP samples were collected each month, with sampling dates properly scheduled between the 10th and 20th of each month, from May 2022 to April 2023. At the CG site, TSP was collected using a high-volume air sampler (Model 120H, Kimoto Electric Co., Japan) operating at 600 L min^{-1} with glass fiber filters (GFFs; Advantec GA-55, 203 × 254 mm). At NVC, a high-volume sampler (Model HV-500R, Sibata Scientific Technology Ltd, Japan) operated at 500 L min^{-1} using GFFs (Advantec; 110 mm diameter). The flow rate accuracy of both sampling instruments was lower than ±5% of the set value, as specified by the manufacturers. All filters were pre-combusted at 400 °C for 8 hours to eliminate residual Hg. The filters were conditioned at 25 ± 2 °C and 40 ± 5% RH for 48 hours before and after sampling. The samples were stored at −20 °C until analysis. Field blanks were prepared, stored, and analyzed following the same protocol to assess potential contamination during sampling and handling. All procedures followed strict QA/QC protocols, including the use of field and laboratory blanks throughout the campaign. Detailed protocols for filter preparation and sample handling are described in previous studies.[18,23,33]

2.2. Mercury and elemental analysis

The concentrations of Hg in GFF samples collected in this study were analyzed at the laboratory of Dr Guey-Rong Sheu, National Central University, Taiwan. Total Hg was quantified using a MA-

3 Solo thermal decomposition analyzer (Nippon Instruments Corporation, Japan) in accordance with USEPA Method 7473, a widely adopted protocol for Hg determination.[18,34,35] The thermal protocol involved an initial heating at 350 °C to remove moisture and volatile organics, followed by a ramp to 850 °C to decompose and release Hg. Gaseous Hg was transported to a gold amalgamation trap, thermally desorbed at 600 °C, and quantified by atomic absorption spectrometry (AAS). Monthly blank values were subtracted to obtain PBM concentrations. Method blanks were < MDL (0.05 ng), with liquid standard recoveries of 99 ± 3% (n = 31). Certified reference materials (NIST SRMs 1648a and 2685c) showed recoveries of 99.8 ± 7.2% and 95.7 ± 3.0%, respectively. These results confirm the method's high precision and analytical reliability. The operational principles and standard QA/QC procedures of the analytical method have been thoroughly documented in previous literature.[18]

Elemental analysis was conducted *via* wet acid digestion followed by inductively coupled plasma mass spectrometry (ICP-MS). 20 elements (Al, As, Ba, Ca, Cd, Co, Cr, Cu, Fe, K, Mg, Mn, Ni, Pb, Sb, Se, Sr, Ti, V, and Zn) were quantified according to U.S. EPA Methods 6020B and 200.8 (Rev. 5.4). Samples were digested using a 2 : 1 (v/v) mixture of HNO_3 and HCl in Teflon vessels, employing microwave-assisted digestion.[23,36] The digested solutions were filtered through 0.45 μm PTFE membranes and analyzed using an Agilent 7700× ICP-MS system (Agilent Technologies, USA). Analytical accuracy was validated with the certified reference material SRM 1684a, achieving recovery rates between 80% and 120% for all 20 elements. Reagent blanks were included to control contamination, and blank values were subtracted to obtain corrected concentrations. Further instrumentation and analytical details are available in our previous study.[23] In this study, elemental data were mainly incorporated into the GAM framework as predictor variables to identify potential drivers of PBM variability rather than to explore the contribution to TSP sources.

In addition, meteorological variables, including temperature (T) and relative humidity (RH), were recorded at sampling sites. Planetary boundary layer (PBL) height and surface-level $PM_{2.5}$ concentration data were derived from the MERRA-2 (Modern-Era Retrospective analysis for Research and Applications, Version 2) reanalysis, which assimilates satellite observations from infrared, microwave, and GPS radio occultation sources.[37,38] A full system description is available in Buchard *et al.*[39] In addition, this study employs the HYSPLIT (Hybrid Single-Particle Lagrangian Integrated Trajectory) model to analyze the backward trajectories of air masses to two study areas. Five-day backward trajectory simulations were conducted for each month within the study period, aiming to identify the origins and movement patterns of the air masses to these locations.[40,41]

2.3. Building the GAM model

In this study, a GAM was used to investigate the relationships between PBM concentrations and chemical elements, as well as meteorological variables. The GAM offers a straightforward and interpretable model for representing the associations between a dependent variable and independent variables.[42] Specifically, the model is expressed as follows:

$$g(\mu_i) = X_i\theta + f_1(x_{1i}) + f_2(x_{2i}) + \ldots + f_n(x_{ni}) + \xi_i \quad (1)$$

where i denotes the ith observation, g is the link function, and μ_i represents the expected value of the dependent variable, defining the relationship between the linear predictor on the right-hand side of eqn (1) and the dependent μ_i. The term $X\theta$ corresponds to the parametric component of the model, capturing the relationship with independent variables characterized by linear relationships. The function $f(x)$ denotes the smooth term associated with nonlinear predictors.

The model construction procedure was carried out in the following steps.

2.3.1 Step 1: data preparation. The dataset used in this study was split into two subsets corresponding to the two monitoring locations. Each sample record includes the concentrations of PBM and 20 elements (Al, As, Ba, Ca, Cd, Co, Cr, Cu, Fe, K, Mg, Mn, Ni, Pb, Sb, Se, Sr, Ti, V, and Zn) in TSP alongside three meteorological variables: T (°C), RH (%), and PBL (m). Precipitation was not included as a predictor in the GAM model due to the lack of high-resolution data for the entire study period and its strongly discontinuous distribution, which reduces model stability. Similarly, other meteorological parameters (*i.e.*, wind speed, wind direction, and atmospheric pressure) were excluded due to data discontinuity and incomplete coverage across the study period. All elemental and meteorological datasets were subjected to standardized quality control procedures. Outliers beyond ±2.5 standard deviations were capped at the respective thresholds.

2.3.2 Step 2: variable selection. To evaluate the normality of the input data, the Shapiro–Wilk test was employed to assess the conformity of each variable to a Gaussian distribution. Details of the test outcomes and the corresponding transformations applied to approximate normality prior to inclusion in the GAM model are provided in Table S1. Penalized cubic regression splines were utilized to smooth the continuous predictors, offering a flexible yet controlled means of capturing nonlinear relationships while minimizing the risk of overfitting.[26,43] Model optimization was guided by generalized cross-validation (GCV), which balances model complexity with predictive performance.[28] Predictor significance was evaluated using p-values, serving as diagnostic metrics for model refinement. The initial full model included all candidate variables, followed by iterative removal of non-significant terms based on their statistical relevance.[26–28]

2.3.3 Step 3: model evaluation. To rigorously evaluate the predictive performance and generalizability of the GAM constructed for the NVC and CG datasets, a 10-fold cross-validation procedure was implemented. This approach is widely recognized in statistical learning,[44] particularly in GAM applications,[43,45] and is increasingly employed in environmental and ecological modeling.[46–48] Each dataset was randomly divided into 10 equal subsets. In each iteration, 9 subsets were used to train the model, while the remaining subset was used for validation. This process was repeated 10 times, ensuring that each

subset served as the validation set once. Model performance in each fold was quantified using the coefficient of determination (R^2), and the mean R^2 across all folds was reported as a robust indicator of the predictive capability of the model.[46] In addition to assessing the adequacy of model assumptions and supporting the validity of inference, diagnostic checks were conducted, including quantile–quantile (Q–Q) plots to evaluate the normality of residuals and autocorrelation function (ACF) plots to examine residual independence (Wood, 2017).

3 Results and discussion

3.1. Characterization of PBM data

Between May 2022 and April 2023, a total of 192 TSP samples were collected from two monitoring sites in HCMC: 97 samples from NVC (urban) and 95 samples from CG (suburban). Meteorological conditions were generally similar between the two suburban sites (*t*-test, $p > 0.05$), with a mean T of 29.0 ± 1.2 °C at NVC and 30.9 ± 1.7 °C at CG, and average RH values of 73.6 ± 6.8% and 69.4 ± 5.3%, respectively. In contrast, PBM concentrations displayed marked spatial variation. The mean PBM concentration at NVC was 59.81 ± 29.15 pg m^{-3}, more than twice the level observed at CG, which averaged 26.4 ± 9.59 pg m^{-3}. This disparity highlights the stronger influence of urban emissions (*i.e.* anthropogenic emissions) on PBM levels within the city center.

Table 1 compares the PBM level in HCMC to those at other sites worldwide. In general, PBM concentrations in HCMC were considerably lower than those reported in several heavily industrialized cities.[19,49,50] For instance, Beijing, China, reported mean levels of 210.1 ± 146.2 pg m^{-3}, approximately 3.5 times higher than those in HCMC.[50] Similarly, Kathmandu, Nepal, recorded concentrations of 850.5 ± 926.8 pg m^{-3}, exceeding HCMC levels by *a* factor of 14 (Guo *et al.*, 2021). Urban centers in developed regions such as Detroit, USA (20.8 ± 30 pg m^{-3}) and Seoul, South Korea (23.9 ± 19.6 pg m^{-3}) also reported higher/comparable values, respectively.[51,52] Comparable trends were observed in Shanghai, China (560 ± 220 and 330 ± 90 pg m^{-3};[49]), and Xi'an, China (640 ± 540 pg m^{-3};[53]). These elevated PBM concentrations have been attributed to emissions from coal combustion, metallurgical activities, and other fossil fuel-related sources.[49,53] Despite its status as a major economic hub, HCMC (particularly NVC) appears to experience relatively limited direct impact from such heavy industrial activities compared to other megacities.

Suburban comparisons also reveal important contrasts. For example, Xiamen, China, reported PBM concentrations approximately 6.7 times higher than those at CG.[54] Dhulikhel, Nepal, recorded levels of 108.7 ± 86.2 pg m^{-3}, about four times those measured at CG.[19] Similarly, PBM levels reported at Zabrze, Poland (65.5 ± 53.7 pg m^{-3}) also exceeded the concentrations at CG, highlighting regional variation in emission sources and atmospheric processes.[55,56] In contrast, the concentration observed at CG (26.4 ± 9.59 pg m^{-3}) is comparable to or higher than those in cleaner or less industrialized coastal settings such as Nova Scotia, Canada (2.32 ± 3.09 pg m^{-3}), Beltsville, USA (8.6 ± 56.8 pg m^{-3}), a high mountain in central Taiwan (3.1 ± 8.5 pg m^{-3}), Taoyuan City, Taiwan (18.7 ± 86.8 pg m^{-3}), and Okinawa, Japan (2.6 ± 3.6 pg m^{-3}) (Table 1).[3,5,17,56,57] These comparisons indicate the relatively moderate level of PBM at CG, suggesting limited influence from heavy industrial activities and reflecting a suburban emission profile distinct from urban-industrialized regions. It is worth noting that the comparisons of PBM concentrations (Table 1) were derived from measurements based on different particle size fractions (*i.e.*, TSP, PM_{10}, and $PM_{2.5}$). Consequently, certain variability is inevitable due to the size-dependent partitioning behavior of mercury.[58] Moreover, distinct physical and chemical characteristics associated with each particle size fraction may further contribute to the observed variations in PBM levels.

Fig. 1 illustrates the relative distribution of elemental composition in TSP collected from urban and suburban

Table 1 Comparison of PBM concentrations (pg m^{-3}) in samples with values reported in other countries worldwide

Site	Size	Type	Year	PBM (pg m^{-3})	References
NVC, Vietnam	TSP	Urban	2022–2023	59.81 ± 29.15	This study
CG, Vietnam	TSP	Suburban	2022–2023	26.4 ± 9.59	This study
Beijing, China	TSP	Urban	2016–2017	210.1 ± 146.2	50
Kathmandu Valley, Nepal	TSP	Urban	2013–2014	850.5 ± 926.8	19
Shanghai, China	TSP	Urban	2004–2006	560 ± 220, 330 ± 90 (2 sites)	49
Xi'an, China	TSP	Urban	2010–2013	640 ± 540	53
Detroit, USA	$PM_{2.5}$	Urban	2006	20.8 ± 30	51
Seoul, Korea	$PM_{2.5}$	Urban	2005–2006	23.9 ± 19.6	52
Xiamen, China	TSP	Suburban	2012–2013	174.1 ± 160.9	54
Dhulikhel, Nepal	TSP	Suburban	2018	108.7 ± 86.2	19
Okinawa, Japan	$PM_{2.5}$	Suburban	2009–2018	2.6 ± 3.6	17
Zabrze, Poland	TSP	Suburban	2013	65.5 ± 53.7	55
Zabrze, Poland	PM_{10}	Suburban	2013	63.6 ± 53.0	55
Nova Scotia, Canada	$PM_{2.5}$	Suburban	2010–2011	2.32 ± 3.09	100
Beltsville, Maryland, USA	$PM_{2.5}$	Suburban	2007–2015	8.6 ± 56.8	56
High mountain in central Taiwan, Taiwan	$PM_{2.5}$	Suburban	2009–2016	3.1 ± 8.5	3
Taoyuan city, Taiwan	$PM_{2.5}$	Suburban	2017–2018	18.7 ± 86.8	5

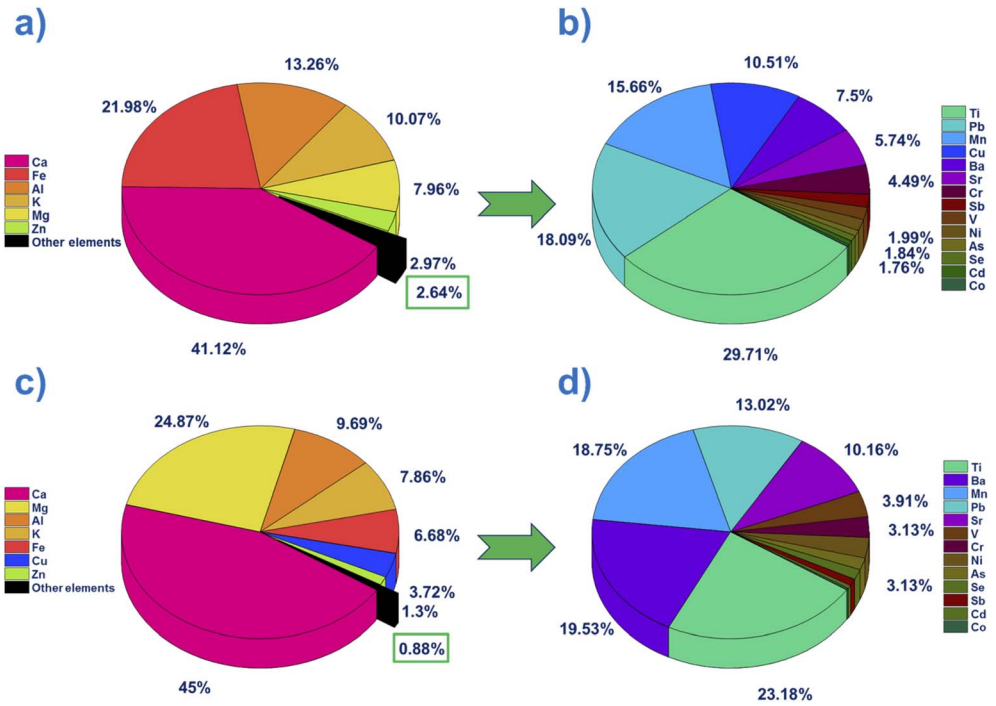

Fig. 1 Pie charts illustrating the percentage (%) of elements TSP samples collected from urban and suburban areas: (a) and (c) show major elements in urban and suburban areas, respectively; (b) and (d) show trace elements in urban and suburban areas, respectively.

environments. In the urban site, Ca was the most dominant element, accounting for 41.12%, followed by Fe (21.98%), Al (13.26%), K (10.07%), and Mg (7.96%) (Fig. 1a). This compositional profile indicates a predominant influence from crustal and anthropogenic contributions, particularly construction, vehicular emissions, and resuspended road dust, characteristic of densely populated urban areas.[18,30,36] The elevated levels of Fe and Al indicate mineral dust inputs, while K and Mg may reflect inputs from biomass burning and soil-derived particles.[8,23,59] Additionally, trace elements such as Zn (2.97%) and Cu (10.51%), found within the category of other elements, also suggest the influence of industrial activities or traffic-related sources.[60–62] Conversely, in the suburban area, although Ca remained the dominant element (45%), Mg emerged as the second most abundant at 24.87%, surpassing Fe (6.68%) (Fig. 1c). This shift suggests a different source profile, potentially related to greater vegetation cover, proximity to the coast, lower human activity intensity, and reduced construction emissions.[32,36,63] Al (9.69%) and K (7.86%) also contributed significantly, along with Cu (3.72%) and Zn (1.3%), which may originate from local anthropogenic activities such as agricultural practices, domestic combustion, or long-range atmospheric transport.[8,23,64]

The distribution of trace elements in TSP at the urban and suburban areas shows distinct differences in the distribution and relative abundance of elements between urban and suburban areas. In the urban area, elements such as Pb (18.09%), Mn (15.66%), and Cu (10.51%) dominate (Fig. 1b), reflecting the influence of anthropogenic activities, particularly emissions from traffic, industrial activities, and construction.[65–67] The correlation analysis among the measured elements was conducted to explore potential associations and shared origins (Tables S2 and S3). Meanwhile, strong correlations among transition metals (*i.e.*, Cr, Mn, and Co) further confirm their common anthropogenic origin ($r = 0.82$–0.91; $p < 0.05$). Likewise, the significant associations between Pb–Cd ($r = 0.84$), As–Se ($r = 0.79$), As–Cd ($r = 0.79$), and Cd–Sb ($r = 0.78$) suggest concurrent emissions from combustion sources and industries using heavy metals.[23,32,36] In contrast, in the suburban area, elements such as Ti (23.18%) and Mn (18.75%) are more prominent (Fig. 1d), indicating a greater influence from natural sources such as soil dust and vegetation.[23,32] The moderate correlations among crustal elements, for instance, Al–K ($r = 0.55$), Al–Ti ($r = 0.53$), and Al–Ca ($r = 0.52$), further confirm the predominance of soil-derived sources. Meanwhile, the significant correlations among Fe–Mn ($r = 0.69$), Ti–Mn ($r = 0.74$), Zn–Fe ($r = 0.60$), and Zn–Mn ($r = 0.51$) likely indicate the influence of anthropogenic activities, possibly traffic-related emissions (Table S3). Additionally, Pb (13.02%) is present at lower levels, indicating less contribution from industrial emissions compared to the urban area.[23,32,36] These differences illustrate spatial variability in elemental composition between the two environments, suggesting differences in population density and surrounding land use characteristics.[32,63,68] These observations are crucial for understanding the behavior of PBM, as the chemical environment in which PBM exists can influence its transformation, transport, and potential health impacts.[11,18,69] Therefore, characterizing elemental distribution patterns is a key foundation for interpreting PBM dynamics in complex urban-suburban transitions.

3.2. Seasonal variation and potential driving factors

Fig. 2 reveals a pronounced seasonal pattern of PBM concentrations at both urban and suburban sites in HCMC. During the major rainy season (July–September), mean PBM concentrations were lower, averaging 38.5 ± 12.4 pg m^{-3} at NVC and 19.8 ± 10.7 pg m^{-3} at CG. In contrast, the major dry season (November–February) exhibited elevated levels at the urban site (109.0 ± 50.9 pg m^{-3}) and the suburban site (40.6 ± 22.2 pg m^{-3}). The seasonal variation in PBM concentrations observed in both urban and suburban sites in HCMC reflects the combined influence of rainfall-driven removal and seasonal air mass transport dynamics.[18,23,32] During the rainy season, frequent and intense rainfall events associated with the Southwest monsoon promote efficient wet scavenging of PBM, resulting in generally lower concentrations. Rainfall facilitates the removal of PBM, especially in tropical environments where convective systems are prevalent.[4,14,18] In contrast, during the dry season, limited rainfall reduces atmospheric cleansing, allowing PBM to accumulate in the boundary layer, resulting in an elevation of PBM levels. In addition, meteorological parameters such as T and RH remained relatively constant across seasons ($p > 0.1$, ANOVA), suggesting that local meteorological variability had limited direct influence on PBM seasonal dynamics.

Furthermore, seasonal variations in prevailing air mass transport patterns, governed by the East Asian monsoon system, play a critical role in shaping atmospheric composition in HCMC.[32,33,70] Results from backward trajectory analyses (Fig. S2 and S3) indicate that during the dry season, air masses predominantly originate from the northeast, possibly originating from highly industrialized regions across continental East Asia.[14,71,72] These air masses could carry high PBM levels, enhancing background PBM levels across both urban and suburban sites in HCMC.[5,17,70] In contrast, during the rainy season, the sampling sites are primarily influenced by southwesterly air masses originating over the ocean (Fig. S2 and S3), which transport relatively clean maritime air to HCMC. Similar seasonal atmospheric Hg trends linked to continental outflow have been reported across East Asia, including Taiwan, Japan, South Korea, and Vietnam.[5,17,70,73]

Notably, during the rainy season, a pronounced difference in PBM concentrations was observed between the urban and suburban sites in June, with the NVC site recording a seasonal maximum of 76.5 ± 29.5 pg m^{-3}, approximately 64% higher than its rainy season mean value (Fig. 2). In contrast, no corresponding peak was detected at the CG site (Fig. 2). Analysis of backward trajectories and surface $PM_{2.5}$ revealed comparable air mass origins for both sites during this period, suggesting that long-range atmospheric transport was not the primary contributor to the elevated PBM levels at NVC (Fig. S2 and S3). Results from surface $PM_{2.5}$ from MERRA-2 further support this conclusion (Fig. S4). The absence of a similar increase at the suburban site supports the interpretation that local accumulation processes, likely driven by stagnant meteorological conditions, predominated at the urban site.[32,33] This interpretation is further supported by meteorological data, which show that June experienced the lowest mean wind speed of the season (1.1 m s^{-1}), considerably lower than values recorded in other months (1.5–1.7 m s^{-1}), favoring the buildup of air pollutants. In summary, the seasonal variability of PBM in HCMC is governed by a complex interplay of local accumulation processes, monsoonal shifts in prevailing air mass origin, and regional-scale pollutant transport. While local emissions dominate during stagnant conditions in the wet season, transboundary transport becomes increasingly significant during the dry season, highlighting the importance of considering both local and regional scales in atmospheric Hg management strategies.

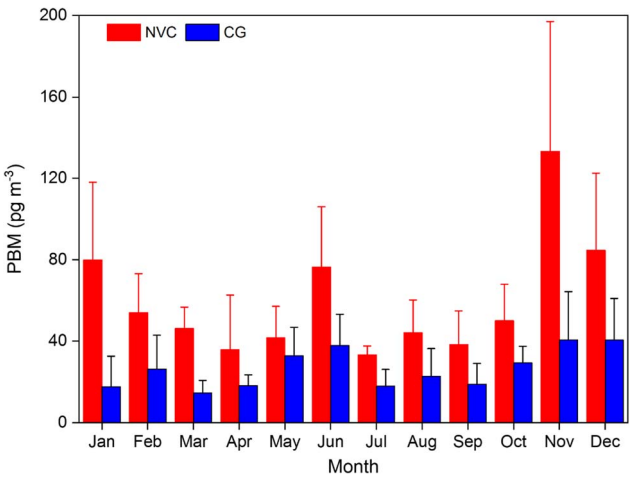

Fig. 2 Monthly variation of PBM concentration (pg m^{-3}) at two sites, Nguyen Van Cu and Can Gio, from May 2022 to April 2023.

3.3. Analysis and evaluation of GAM performance

Based on the variable selection results presented in Table S4, a total of 19 independent variables (PBL height and 18 elements) were retained for the NVC dataset, while only 3 variables (PBL, T, and Zn) were retained for CG ($p < 0.05$, summary function). Model performance metrics are summarized in Table S5. The GAM indicated strong correlations between the selected predictors and PBM concentrations, with R^2 reaching 90.8% for NVC and 94.5% for CG, indicating robust initial fits.[28,43,74] However, the explanatory power of the models, as measured by adjusted R^2, differed markedly: 0.73 at NVC and only 0.32 at CG (Table S5). The adjusted R^2 of 0.73 at NVC indicates a strong and reliable model performance, suggesting that the selected predictors captured most of the variability in PBM concentrations at this site. In contrast, the much lower adjusted R^2 at CG implies a weaker model fit, potentially due to unaccounted site-specific factors or greater variability in local conditions. This contrast suggests a reduced ability to generalize the influencing factors of PBM concentrations in suburban environments.[75,76]

The higher explanatory capacity of the NVC model can be attributed to the broader spectrum of input variables, which likely captured key emission sources and meteorological influences. In contrast, the limited predictor set for CG constrained the model's ability to represent PBM variability. Comparative assessment with prior studies further highlights the improved

performance of the current urban model. The statistical model explained 87.7% of the variance in PBM concentrations, with the adjusted R^2 reaching 0.73 at the NVC site, indicating superior performance compared to the model of TGM in the Beijing-Tianjin-Hebei region, which achieved an adjusted $R^2 = 0.62$ and explained 63.2% of the variability.[28] In contrast, at the CG site, the statistical model showed a considerably lower predictive capacity, explaining 41.6% of the variance in PBM concentrations, with the adjusted R^2 reaching 0.32, consistent with the findings of Wu *et al.*,[27] where the model explained 56.7% of the TGM variability (adjusted $R^2 = 0.551$). It should be noted that our model was developed for PBM, while the referenced studies modeled TGM, which may inherently differ in their atmospheric behavior, influencing model sensitivity and explanatory capacity.

These results emphasize the critical importance of incorporating a diverse array of explanatory variables. The limited inclusion of local environmental indicators (*e.g.*, land use, vegetation cover, and potential emission sources) may have further hindered model performance at CG.[25,68,77] Diagnostic analyses from Fig. S5 and S6 indicate that both GAM models at the NVC and CG sites satisfy key statistical assumptions and are well-suited to the environmental characteristics of each location. At NVC, the residuals follow a normal distribution and are homogeneously dispersed around zero, and the predicted values align closely with observations, demonstrating high model accuracy and strong predictive capacity. At CG, the residuals also exhibit a normal distribution, with a symmetric histogram and Q–Q plot, and no systematic bias across fitted values. Overall, both models are statistically reliable and highlight the flexibility of GAMs in analyzing PBM across contrasting environmental settings.[43,78,79]

3.4. Relationship analysis results

Fig. 3 and S8 show the nonlinear relationships between PBM and other parameters (*i.e.* elements and meteorology) at the NVC site, revealing complex interactions between emission sources and atmospheric processes. Several crustal (*e.g.*, Al, Ti; Fig. S8) and anthropogenic elements (*e.g.*, Cd, Co, Cr, Cu, Pb, and Sb) exhibited statistically significant positive associations with PBM levels, suggesting their potential role in PBM-enriched source sectors such as traffic-related emissions, coal combustion, and industrial activities at the sampling site.[18,23,32] This finding aligns with previous GAM-based studies, where key emission sectors (*e.g.*, cement and power plants) exhibited significant relationships with Hg levels, emphasizing the dominant influence of anthropogenic drivers on atmospheric Hg variation.[27,28] By contrast, the PBL showed an inverse relationship with PBM (Fig. 3), consistent with enhanced vertical mixing and dilution under higher PBL conditions.[30,54] Similar findings were reported by Wu *et al.*[28] in Beijing, China, indicating that elevated PBL contributed to reductions in atmospheric Hg concentrations due to improved atmospheric dispersion.

Some elements (*i.e.*, As, Ba, Fe, Mn, Ni, and Se) showed threshold-dependent nonlinearities. For instance, As and Ba displayed negative relationships with PBM at lower concentrations (<0.4 ng m^{-3} and <9 ng m^{-3}, respectively; Fig. S8) but transitioned to positive relationships above these thresholds, indicating potential shifts in dominant sources or physicochemical partitioning behavior at higher loadings. These turning points may reflect saturation kinetics or source mixing, where low concentrations are dominated by background or natural sources, whereas elevated levels originate from combustion-related emissions.[10,12,80,81] Moreover, elements such as K, Sr, V, and Zn exhibited highly nonlinear trends with multiple inflection points (Fig. S8), suggesting their involvement in complex multiphase reactions or simultaneous contributions from diverse sources (*e.g.*, biomass burning, traffic, and re-suspension processes). For instance, the GAM-based spline revealed that Zn exhibited a positive association with PBM concentrations at lower levels (up to ~125 ng m^{-3}),

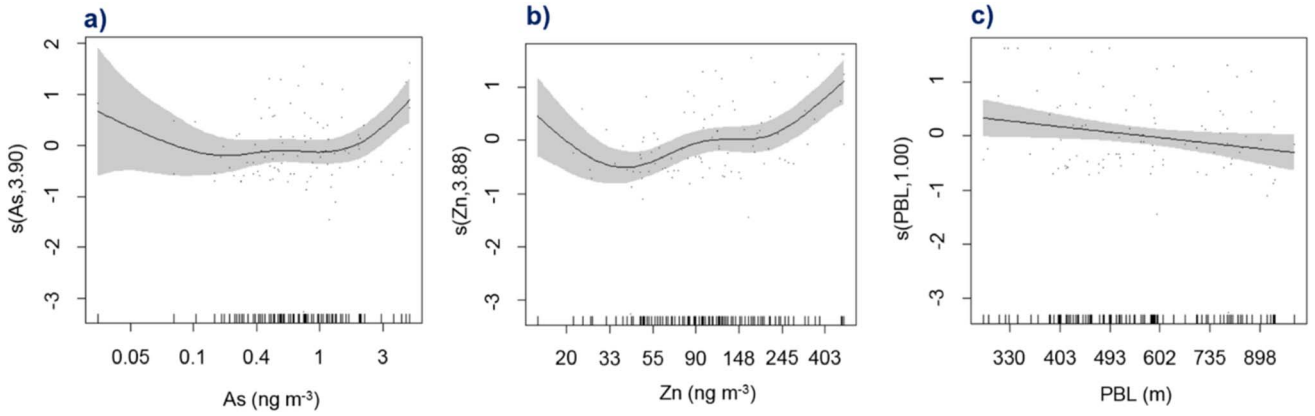

Fig. 3 Spline plots illustrate the relationships between PBM concentration and elemental concentrations at the NVC monitoring site: (a) As, (b) Zn, and (c) PBL – the meteorological parameter. The *y*-axis represents the spline values of PBM as a function of each independent variable, and the *x*-axis corresponds to the observed values of each independent variable. The solid line indicates the fitted spline, while the shaded area around it represents the 95% confidence interval for the predicted response. Tick marks on the *x*-axis show the distribution of the data points. The number in parentheses in each *y*-axis label denotes the estimated degrees of freedom (EDF). Dots in the plots represent residual values.

after which the relationship plateaued or slightly declined (Fig. 3). This trend may reflect atmospheric saturation effects, particle-phase condensation limitations, or increased partitioning into coarse-mode particles at higher Zn concentrations, which may be less efficient at binding PBM.[16] Additionally, under humid atmospheric conditions, Zn may facilitate heterogeneous reactions on particle surfaces or act as a catalyst in redox transformations of oxidized Hg.[82,83] These findings imply the dual role of Zn as both a source tracer and a potential participant in secondary atmospheric processes influencing PBM formation and stability. Given the ubiquitous presence of traffic emissions in urban environments, the role of Zn as a proxy for this source category highlights the importance of traffic-related activities as a critical and persistent contributor to atmospheric Hg cycling.

At the CG site, meteorological variables, including T and PBL, showed similarly complex effects on PBM (Fig. 4). T showed a nonlinear association with PBM (Fig. 4a), characterized by a negative response between 26 and 30 °C and a slight increase above 30 °C. The PBM-T relationship is inherently complex, as T controls the gas–particle partitioning of Hg(II), and lower temperatures favor particle-bound fractions, whereas higher temperatures enhance gaseous forms.[9,12] Moreover, temperature variations may reflect shifts in air mass origins (*e.g.*, land-sea breeze), further influencing PBM levels.[12,84,85] The inverse relationship between the PBL and PBM became evident above 330 m, reinforcing the role of boundary layer dynamics in pollutant dilution. Notably, Zn at CG revealed a concentration-dependent relationship with PBM, positively correlated below 125 ng m^{-3} but negatively correlated beyond this threshold. This may indicate distinct PM binding capacities or interactions under varying atmospheric chemical regimes. Similar concentration-reversal effects of RH on TGM were reported by Wu *et al.*,[28] where RH >80% enhanced aqueous phase reduction processes and TGM re-emission, further illustrating the nonlinear behavior of Hg species in atmospheric systems.

In general, these results indicate the multifactorial nature of PBM variability, governed by a combination of potential emission source profiles and meteorological controls at both urban and suburban sites in HCMC. However, it should be acknowledged that several nonlinear relationships revealed in the GAM remain partially unexplained, particularly those involving threshold-dependent behaviors and inflection points. These complexities may stem from unmeasured variables, insufficient temporal resolution, or limitations in chemical speciation data. Consequently, our ability to fully interpret the integrated influence of chemical and meteorological predictors on PBM remains constrained.

3.5. Contribution rates of independent variables, implications for potential driving factors on PBM variabilities

Table S6 shows the proportional contributions of factors influencing PBM concentration variability at NVC and CG sites, as determined by the VarImp function in the GAM model.[25,27,28] The relative importance of independent variables reveals striking contrasts between the two monitoring environments, highlighting the distinct roles of emission sources and meteorological controls in shaping PBM dynamics.

At the CG suburban site, meteorological conditions overwhelmingly dominated PBM variability, collectively accounting for 78.7% of the total variance (Fig. 5). Among these, T alone explained 60.8%, consistent with a strong positive, though nonlinear, association observed in the GAM spline. In addition, the PBL contributed 17.9% to PBM variation, reflecting the dispersive capacity of elevated mixing layers to dilute PBM concentrations, as noted in previous studies.[32,33] These results indicate that in areas with limited direct emissions, PBM levels are primarily modulated by atmospheric dynamics.

In contrast, meteorological factors played a minor role at the urban NVC site, explaining only 1.2% of the variance (Fig. 5). This suggests that urban PBM levels are largely dominated by localized anthropogenic emissions. Indeed, anthropogenic sources contributed over 87.7% of the PBM variability at NVC, reflecting the complex contribution of combustion, industrial, and traffic-related emissions in a densely populated setting. Among combustion-related sources, several elements showed high contributions to PBM at NVC, including Pb (8.8%), V (8.3%), Cd (5.5%), and As (5.6%), all commonly associated with

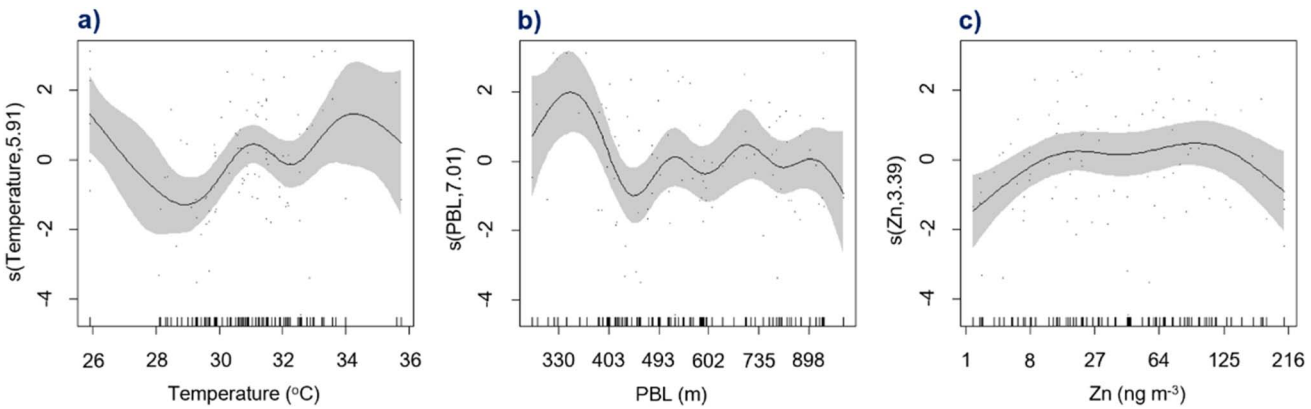

Fig. 4 Spline plots illustrate the relationships between PBM concentration and elemental concentrations at the CG monitoring site: (a) Temperature, (b) PBL, and elemental concentration: (c) Zn.

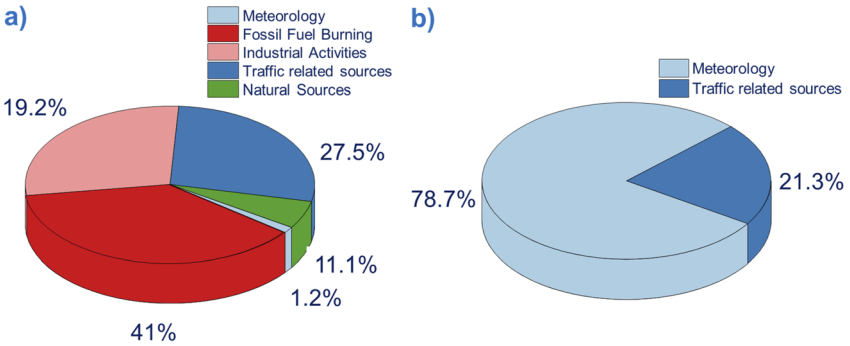

Fig. 5 Source category contributions to PBM variability at the two sampling sites (a) urban and (b) suburban.

fossil fuel burning.[86,87] Pb and V are particularly indicative of the use of heavy oils and fossil fuels in both transportation and industrial processes.[36,59,65] K (4.6%), Se (4.6%), and Sb (3.6%) also played significant roles within the combustion-related source group, although they are often considered to originate from mixed sources. K is a well-known tracer of biomass burning, commonly found in plant ash and produced from the combustion of wood, crop residues, or other organic materials.[88,89] The prominent presence of K suggests the possible influence of local open burning or resuspension of ash-derived dust within the urban environment. In contrast, Se is typically found in emissions from heavy oil and coal combustion, particularly from power plants and industrial facilities using fossil fuels.[90–92]

These elements also exhibited strong and significant positive associations in GAM splines, suggesting their diagnostic importance in PBM variation. In addition, industrial-related elements, including Sr (8.9%), Ni (5.8%), Co (3.9%), and Ba (0.6%), were also important predictors at NVC. These originate from diverse industrial activities such as steel production, alloy and battery manufacturing, and pigment and flame-retardant use.[36,61,93,94] Although anthropogenic influences were predominant, natural sources contributed a non-negligible 11.1% to the PBM variation at the NVC site. Specifically, elements such as Ti (5.4%), Fe (4.2%), and Al (1.5%), commonly associated with crustal material, re-suspended soil dust, or biogenic emissions, were linked to natural origins.[36,63] These elements likely reflect background processes such as wind-driven dust resuspension, long-range transport of mineral aerosols, and interactions with natural surfaces. While their contributions were smaller than those from combustion or industrial sources, they provide a stable background signal and may influence PBM behavior through surface reactivity or chemical partitioning mechanisms. Therefore, the combined effect of both anthropogenic and natural inputs should be considered in assessing PBM dynamics and developing targeted control strategies.

Furthermore, non-combustion traffic-related elements (*i.e.* Cr, Mn, Cu, and Zn) accounted for 27.5% of PBM variability at NVC. These metals are predominantly released from brake and tire wear, engine oil leakage, and road dust re-suspension.[18,62,95] At the CG site, Zn was the only elemental contributor to PBM variability (21.3%), suggesting that localized emissions from traffic-related sources remain relevant even in suburban settings. This is consistent with previous findings indicating that Zn can persist regionally due to its semi-volatile behavior and association with fine-mode aerosols.[96,97]

In general, the distribution of PBM drivers across the two sites reflects fundamental environmental contrasts. While the urban NVC site is characterized by intensive anthropogenic emissions from multiple sectors, the suburban CG site is primarily governed by meteorological processes, with localized Zn emissions playing a secondary role. These insights support the development of site-specific air quality control strategies: urban areas should prioritize emission mitigation (especially from traffic and fuel combustion), whereas regional management must consider atmospheric mixing and temperature-driven re-emission processes.

4 Conclusion

This study presents the first year-long dataset of PBM at urban and suburban sites in HCMC, providing novel insights into PBM dynamics in a tropical SEA megacity. Distinct spatial and temporal variations were observed, with higher mean PBM concentrations at the urban site (59.81 ± 29.15 pg m^{-3}) compared to the suburban site (26.4 ± 9.59 pg m^{-3}). Seasonal trends revealed elevated levels during the dry season. By applying a GAM, this study successfully quantified the nonlinear influences of chemical and meteorological parameters on PBM. The GAM explained 87.7% of PBM variance at the urban site, compared to 41.6% at the suburban site, indicating its greater predictive power in emission-rich environments. At the urban site, anthropogenic emissions dominated PBM variability, with industrial and combustion-related elements such as As, Cd, Pb, V, K, Se, and Sb contributing 41%. In contrast, PBM at the suburban site was primarily modulated by temperature (60.8%), Zn (21.3%), and planetary boundary layer height (17.9%), reflecting the stronger role of atmospheric processes in low-emission areas. The findings implied the efficacy of the GAM in unraveling complex PBM–environment interactions, offering a robust framework for source apportionment. Importantly, the observed site-specific drivers suggest that urban areas should prioritize emission controls targeting traffic and industrial sectors, while suburban management strategies

should consider meteorological influences and regional transport mechanisms. Overall, this work provides critical evidence for tailoring Hg mitigation policies to local environmental contexts and emphasizes the utility of flexible, data-driven modeling approaches in advancing atmospheric Hg research and air quality management. On the other hand, we acknowledge certain analytical limitations specific to the current study. Upcoming studies should incorporate expanded datasets that integrate higher time-resolution measurements, detailed chemical speciation of PM, and more complete meteorological parameters, together with advanced analytical approaches such as integrated PMF-GAM modeling.[98,99] Such developments will enable a more robust identification of source contributions, thereby improving the mechanistic understanding of PBM dynamics in complex atmospheric environments.

Author contributions

Ly Sy Phu Nguyen: conceptualization, methodology, resources, supervision, and writing – original draft. Duc Thanh Nguyen: methodology, investigation, data curation, and writing – original draft. Le Quoc Hau: investigation, visualization and writing – review and editing. Guey-Rong Sheu: resources, investigation, and writing – review and editing. To Thi Hien: conceptualization and investigation.

Conflicts of interest

The authors declare no conflicts.

Data availability

The data supporting the findings of this study are available from the corresponding author upon reasonable request.

Supplementary information is available. See DOI: **https://doi.org/10.1039/d5ea00094g**.

Acknowledgements

This research is funded by the University of Science, VNU-HCM under grant number T2024-121.

References

1 UNEP, *Global Mercury Assessment 2013: Sources, Emissions, Releases and Environmental Transport, Chemicals Branch*, Geneva, Switzerland, 2013.
2 UN Environment, *Global Mercury Assessment 2018, Chemicals and Health Branch*, Geneva, Switzerland, 2019.
3 L. S. P. Nguyen, L. Zhang, D. W. Lin, N. H. Lin and G. R. Sheu, Eight-year dry deposition of atmospheric mercury to a tropical high mountain background site downwind of the East Asian continent, *Environ. Pollut.*, 2019, **255**, 113128, DOI: **10.1016/j.envpol.2019.113128**.
4 D. Obrist, J. L. Kirk, L. Zhang, E. M. Sunderland, M. Jiskra and N. E. Selin, A review of global environmental mercury processes in response to human and natural perturbations: changes of emissions, climate, and land use, *Ambio*, 2018, **47**, 116–140, DOI: **10.1007/s13280-017-1004-9**.
5 G. R. Sheu, L. S. P. Nguyen, M. T. Truong and D. W. Lin, Characteristics of atmospheric mercury at a suburban site in northern Taiwan and influence of trans-boundary haze events, *Atmos. Environ.*, 2019, **214**, 116827, DOI: **10.1016/j.atmosenv.2019.116827**.
6 L. Zhang, S. Wang, L. Wang, Y. Wu, L. Duan, Q. Wu and X. Liu, Updated emission inventories for speciated atmospheric mercury from anthropogenic sources in China, *Environ. Sci. Technol.*, 2015, **49**(5), 3185–3194, DOI: **10.1021/es504840m**.
7 J. Guo, K. Ram, L. Tripathee, S. Kang, J. Huang, P. Chen and P. S. Ghimire, Study on mercury in PM10 at an urban site in the Central Indo-Gangetic plain: seasonal variability and influencing factors, *Aerosol Air Qual. Res.*, 2020, **20**(12), 2729–2740, DOI: **10.4209/aaqr.2019.12.0630**.
8 L. S. P. Nguyen, H. Y. Huang, T. L. Lei, T. T. Bui, S. H. Wang, K. H. Chi and N. H. Lin, Characterizing a landmark biomass-burning event and its implication for aging processes during long-range transport, *Atmos. Environ.*, 2020, **241**, 117766, DOI: **10.1016/j.atmosenv.2020.117766**.
9 L. S. P. Nguyen, G. R. Sheu, T. C. Hsiao, C. T. Lee, S. C. Chang and N. H. Lin, Relationships between atmospheric mercury and optical properties of spring outflow aerosols from Southeast Asia, *Atmos. Pollut. Res.*, 2021, **12**(10), 101178, DOI: **10.1016/j.apr.2021.101178**.
10 P. A. Ariya, M. Amyot, A. Dastoor, D. Deeds, A. Feinberg, G. Kos and K. Toyota, Mercury physicochemical and biogeochemical transformation in the atmosphere and at atmospheric interfaces: A review and future directions, *Chem. Rev.*, 2015, **115**, 3760–3802, DOI: **10.1021/cr500667e**.
11 S. M. Dunham-Cheatham, S. Lyman and M. S. Gustin, Comparison and calibration of methods for ambient reactive mercury quantification, *Sci. Total Environ.*, 2023, **856**, 159219, DOI: **10.1016/j.scitotenv.2022.159219**.
12 L. S. P. Nguyen, G. R. Sheu, S. C. Chang and N. H. Lin, Effects of temperature and relative humidity on the partitioning of atmospheric oxidized mercury at a high-altitude mountain background site in Taiwan, *Atmos. Environ.*, 2021, **261**, 118572, DOI: **10.1016/j.atmosenv.2021.118572**.
13 Q. Wu, S. Wang, G. Li, S. Liang, C. J. Lin, Y. Wang and J. Hao, Temporal trend and spatial distribution of speciated atmospheric mercury emissions in China during 1978-2014, *Environ. Sci. Technol.*, 2016, **50**(24), 13428–13435, DOI: **10.1021/acs.est.6b04308**.
14 L. S. P. Nguyen, D. W. Lin, N. H. Lin and G. R. Sheu, Temporal changes in atmospheric mercury concentrations at a background mountain site downwind of the East Asia continent in 2006–2016, *Sci. Total Environ.*, 2019, **686**, 1049–1056, DOI: **10.1016/j.scitotenv.2019.05.425**.
15 X. Fu, H. Zhang, X. Feng, Q. Tan, L. Ming, C. Liu and L. Zhang, Domestic and transboundary sources of atmospheric particulate bound mercury in remote areas

of China: evidence from mercury isotopes, *Environ. Sci. Technol.*, 2019, **53**(4), 1947–1957, DOI: 10.1021/acs.est.8b06736.

16 D. Han, J. Zhang, Z. Hu, Y. Ma, Y. Duan, Y. Han and W. Wang, Particulate mercury in ambient air in Shanghai, China: size-specific distribution, gas-particle partitioning, and association with carbonaceous composition, *Environ. Pollut.*, 2018, **238**, 543–553, DOI: 10.1016/j.envpol.2018.03.088.

17 K. Marumoto, N. Suzuki, Y. Shibata, A. Takeuchi, A. Takami, N. Fukuzaki and M. Saito, Long-term observation of atmospheric speciated mercury during 2007-2018 at Cape Hedo, Okinawa, Japan, *Atmosphere*, 2019, **10**(7), 362, DOI: 10.3390/atmos10070362.

18 L. S. P. Nguyen, T. T. Hien, M. T. Truong, N. D. T. Chi and G. R. Sheu, Atmospheric particulate-bound mercury (PBM_{10}) in a Southeast Asia megacity: sources and health risk assessment, *Chemosphere*, 2022, **307**, 135707, DOI: 10.1016/j.chemosphere.2022.135707.

19 J. Guo, C. M. Sharma, L. Tripathee, S. Kang, X. Fu, J. Huang and P. Chen, Source identification of atmospheric particle-bound mercury in the Himalayan foothills through non-isotopic and isotope analyses, *Environ. Pollut.*, 2021, **286**, 117317, DOI: 10.1016/j.envpol.2021.117317.

20 K. Li, D. J. Jacob, H. Liao, L. Shen, Q. Zhang and K. H. Bates, Anthropogenic drivers of 2013-2017 trends in summer surface ozone in China, *Proc. Natl. Acad. Sci. U. S. A.*, 2019, **116**(2), 422–427, DOI: 10.1073/pnas.1812168116.

21 X. Xu, Y. Liao, I. Cheng and L. Zhang, Potential sources and processes affecting speciated atmospheric mercury at Kejimkujik National Park, Canada: comparison of receptor models and data treatment methods, *Atmos. Chem. Phys.*, 2017, **17**(2), 1381–1400, DOI: 10.5194/acp-17-1381-2017.

22 Y. H. Taguchi, *Unsupervised Feature Extraction Applied to Bioinformatics: A PCA Based and TD Based Approach*, Springer Nature, 2024, DOI: 10.1007/978-3-031-60982-4.

23 M. T. Truong, L. S. P. Nguyen, T. T. Hien, T. D. H. Pham and T. T. L. Do, Source apportionment and risk estimation of heavy metals in PM_{10} at a Southern Vietnam megacity, *Aerosol Air Qual. Res.*, 2022, **22**(8), 220094, DOI: 10.4209/aaqr.220094.

24 B. Xu, H. Xu, H. Zhao, J. Gao, D. Liang, Y. Li and G. Shi, Source apportionment of fine particulate matter at a megacity in China, using an improved regularization supervised PMF model, *Sci. Total Environ.*, 2023, **879**, 163198, DOI: 10.1016/j.scitotenv.2023.163198.

25 K. Ravindra, P. Rattan, S. Mor and A. N. Aggarwal, Generalized additive models: building evidence of air pollution, climate change and human health, *Environ. Int.*, 2019, **132**, 104987, DOI: 10.1016/j.envint.2019.104987.

26 S. N. Wood, Stable and efficient multiple smoothing parameter estimation for generalized additive models, *J. Am. Stat. Assoc.*, 2004, **99**(467), 673–686, DOI: 10.1198/016214504000000980.

27 Q. Wu, Y. Tang, S. Wang, L. Li, K. Deng, G. Tang and H. Zhang, Developing a statistical model to explain the observed decline of atmospheric mercury, *Atmos. Environ.*, 2020, **243**, 117868, DOI: 10.1016/j.atmosenv.2020.117868.

28 Q. Wu, Y. Tang, L. Wang, S. Wang, D. Han, D. Ouyang and J. Hu, Impact of emission reductions and meteorology changes on atmospheric mercury concentrations during the COVID-19 lockdown, *Sci. Total Environ.*, 2021, **750**, 142323, DOI: 10.1016/j.scitotenv.2020.142323.

29 J. D. Krug, A. Dart, C. L. Witherspoon, J. Gilberry, Q. Malloy, S. Kaushik and R. W. Vanderpool, Revisiting the size selective performance of EPA's high-volume total suspended particulate matter (Hi-Vol TSP) sampler, *Aerosol Sci. Technol.*, 2017, **51**(7), 868–878, DOI: 10.1080/02786826.2017.1316358.

30 T. T. Hien, N. D. T. Chi, N. T. Nguyen, L. X. Vinh, N. Takenaka and D. H. Huy, Current status of fine particulate matter ($PM_{2.5}$) in Vietnam's most populous city, Ho Chi Minh City, *Aerosol Air Qual. Res.*, 2019, **19**(10), 2239–2251, DOI: 10.4209/aaqr.2018.12.0471.

31 N. D. Dat, L. S. P. Nguyen, T. D. H. Vo, T. Van Nguyen, T. T. L. Do, A. T. K. Tran and N. T. T. Hoang, Pollution characteristics, associated risks, and possible sources of heavy metals in road dust collected from different areas of a metropolis in Vietnam, *Environ. Geochem. Health*, 2023, **45**(11), 7889–7907, DOI: 10.1007/s10653-023-01696-4.

32 T. T. Hien, L. S. P. Nguyen, M. T. Truong, T. D. H. Pham, T. A. Ngan, T. H. Minh and N. T. Nguyen, Spatiotemporal variations of atmospheric mercury at urban and suburban areas in Southern Vietnam megacity: A preliminary year-round measurement study, *Atmos. Environ.*, 2024, **333**, 120664, DOI: 10.1016/j.atmosenv.2024.120664.

33 L. S. P. Nguyen, T. D. H. Pham, M. T. Truong and A. N. Tran, Characteristics of total gaseous mercury at a tropical megacity in Vietnam and influence of tropical cyclones, *Atmos. Pollut. Res.*, 2023, **14**(8), 101813, DOI: 10.1016/j.apr.2023.101813.

34 D. S. McLagan, F. Monaci, H. Huang, Y. D. Lei, C. P. Mitchell and F. Wania, Characterization and quantification of atmospheric mercury sources using passive air samplers, *J. Geophys. Res.:Atmos.*, 2019, **124**(4), 2351–2362, DOI: 10.1029/2018JD029373.

35 J. Zheng, M. Li, B. Tang, W. Luo, Y. Ma, M. Ren and B. Mai, Levels, spatial distribution, and impact factors of heavy metals in the hair of metropolitan residents in China and human health implications, *Environ. Sci. Technol.*, 2021, **55**(15), 10578–10588, DOI: 10.1021/acs.est.1c02001.

36 N. D. Dat, M. T. Truong, L. S. P. Nguyen, A. T. K. Tran, N. M. Duc, T. D. H. Vo and G. R. Sheu, Street dust mercury levels among different land-use categories in Ho Chi Minh City, Vietnam: Source apportionment and risk estimation, *Atmos. Pollut. Res.*, 2023, **14**(1), 101623, DOI: 10.1016/j.apr.2022.101623.

37 R. Gelaro, W. McCarty, M. J. Suárez, R. Todling, A. Molod, L. Takacs and B. Zhao, The modern-era retrospective analysis for research and applications, version 2 (MERRA-2), *J. Clim.*, 2017, **30**(14), 5419–5454, DOI: 10.1175/JCLI-D-16-0758.1.

38 H. Y. Huang, S. H. Wang, W. X. Huang, N. H. Lin, M. T. Chuang, A. M. da Silva and C. M. Peng, Influence of synoptic-dynamic meteorology on the long-range transport of Indochina biomass burning aerosols, *J. Geophys. Res.:Atmos.*, 2020, **125**(3), e2019JD031260, DOI: 10.1029/2019JD031260.

39 V. Buchard, C. A. Randles, A. M. Da Silva, A. Darmenov, P. R. Colarco, R. Govindaraju and H. Yu, The MERRA-2 aerosol reanalysis, 1980 onward. Part II: Evaluation and case studies, *J. Clim.*, 2017, **30**(17), 6851–6872, DOI: 10.1175/JCLI-D-16-0613.1.

40 R. R. Draxler and G. D. Rolph, *HYSPLIT (Hybrid Single-Particle Lagrangian Integrated Trajectory) Model Access via NOAA ARL READY*, NOAA Air Resources Laboratory, Silver Spring, MD, 2013, https://www.arl.noaa.gov/HYSPLIT.php.

41 S. H. Wang, W. T. Hung, S. C. Chang and M. C. Yen, Transport characteristics of Chinese haze over Northern Taiwan in winter, 2005-2014, *Atmos. Environ.*, 2016, **126**, 76–86, DOI: 10.1016/j.atmosenv.2015.11.043.

42 M. Aldrin and I. H. Haff, Generalised additive modelling of air pollution, traffic volume and meteorology, *Atmos. Environ.*, 2005, **39**, 2145–2155, DOI: 10.1016/j.atmosenv.2004.12.020.

43 S. N. Wood, *Generalized Additive Models: an Introduction with R*, Chapman & Hall/CRC, 2017, DOI: 10.1201/9781315370279.

44 T. Hastie, R. Tibshirani, J. H. Friedman and J. H. Friedman, *The Elements of Statistical Learning: Data Mining, Inference, and Prediction*, Springer, New York, 2009, Vol. 2, pp. 1–758.

45 T. J. Hastie, *Generalized Additive Models, Statistical Models in S*, 2017, pp. 249–307.

46 T. Fushiki, Estimation of prediction error by using K-fold cross-validation, *Stat. Comput.*, 2011, **21**, 137–146, DOI: 10.1007/s11222-009-9153-8.

47 Y. Jung, Multiple predicting K-fold cross-validation for model selection, *J. Nonparametric Stat.*, 2018, **30**(1), 197–215, DOI: 10.1080/10485252.2017.1404598.

48 L. A. Yates, Z. Aandahl, S. A. Richards and B. W. Brook, Cross validation for model selection: a review with examples from ecology, *Ecol. Monogr.*, 2023, **93**(1), e1557, DOI: 10.1002/ecm.1557.

49 G. Xiu, J. Cai, W. Zhang, D. Zhang, A. Büeler, S. Lee and P. Zhang, Speciated mercury in size-fractionated particles in Shanghai ambient air, *Atmos. Environ.*, 2009, **43**(19), 3145–3154, DOI: 10.1016/j.atmosenv.2008.07.044.

50 X. Qin, X. Dong, C. Liu, R. Wei, Z. Tao, H. Zhang and Q. Guo, Mass-independent fractionation of mercury stable isotopes reveals atmospheric transport impact on particulate-bound mercury, *Geophys. Res. Lett.*, 2025, **52**(17), e2025GL116080, DOI: 10.1029/2025GL116080.

51 B. Liu, G. J. Keeler, J. T. Dvonch, J. A. Barres, M. M. Lynam, F. J. Marsik and J. T. Morgan, Temporal variability of mercury speciation in urban air, *Atmos. Environ.*, 2007, **41**(9), 1911–1923, DOI: 10.1016/j.atmosenv.2006.10.063.

52 S. H. Kim, Y. J. Han, T. M. Holsen and S. M. Yi, Characteristics of atmospheric speciated mercury concentrations (TGM, Hg(II) and Hg(p)) in Seoul, Korea, *Atmos. Environ.*, 2009, **43**(20), 3267–3274, DOI: 10.1016/j.atmosenv.2009.02.038.

53 H. Xu, J. E. Sonke, B. Guinot, X. Fu, R. Sun, A. Lanzanova and J. Cao, Seasonal and annual variations in atmospheric Hg and Pb isotopes in Xi'an, China, *Environ. Sci. Technol.*, 2017, **51**(7), 3759–3766, DOI: 10.1021/acs.est.6b06145.

54 L. Xu, J. Chen, L. Yang, Z. Niu, L. Tong, L. Yin and Y. Chen, Characteristics and sources of atmospheric mercury speciation in a coastal city, Xiamen, China, *Chemosphere*, 2015, **119**, 530–539, DOI: 10.1016/j.chemosphere.2014.07.024.

55 H. Pyta and W. Rogula-Kozłowska, Determination of mercury in size-segregated ambient particulate matter using CVAAS, *Microchem. J.*, 2016, **124**, 76–81, DOI: 10.1016/j.microc.2015.08.001.

56 X. Ren, W. T. Luke, P. Kelley, M. D. Cohen, R. Artz, M. L. Olson and J. W. Stehr, Atmospheric mercury measurements at a suburban site in the Mid-Atlantic United States: inter-annual, seasonal and diurnal variations and source-receptor relationships, *Atmos. Environ.*, 2016, **146**, 141–152, DOI: 10.1016/j.atmosenv.2016.08.028.

57 L. Poissant, M. Pilote, C. Beauvais, P. Constant and H. H. Zhang, A year of continuous measurements of three atmospheric mercury species (GEM, RGM and Hgp) in southern Quebec, Canada, *Atmos. Environ.*, 2005, **39**(7), 1275–1287, DOI: 10.1016/j.atmosenv.2004.11.007.

58 D. M. Feddersen, R. Talbot, H. Mao and B. C. Sive, Size distribution of atmospheric particulate mercury in marine and coastal atmospheres, *ACPD*, 2012, **12**(6), DOI: 10.5194/acpd-12-14591-2012.

59 X. Li, L. Liu, Y. Wang, G. Luo, X. Chen, X. Yang and X. He, Heavy metal contamination of urban soil in an old industrial city (Shenyang) in Northeast China, *Geoderma*, 2013, **192**, 50–58, DOI: 10.1016/j.geoderma.2012.08.011.

60 T. B. Councell, K. U. Duckenfield, E. R. Landa and E. Callender, Tire-wear particles as a source of zinc to the environment, *Environ. Sci. Technol.*, 2004, **38**(15), 4206–4214, DOI: 10.1021/es034631f.

61 M. Keane, A. Siert, S. Stone and B. T. Chen, Profiling stainless steel welding processes to reduce fume emissions, hexavalent chromium emissions and operating costs in the workplace, *J. Occup. Environ. Hyg.*, 2016, **13**(1), 1–8, DOI: 10.1080/15459624.2015.1072634.

62 J. Sternbeck, Å. Sjödin and K. Andréasson, Metal emissions from road traffic and the influence of resuspension-results from two tunnel studies, *Atmos. Environ.*, 2002, **36**(30), 4735–4744, DOI: 10.1016/S1352-2310(02)00561-7.

63 Z. Bozkurt, O. E. Gaga, F. Taşpınar, A. Arı, B. Pekey, H. Pekey and Ö. Özden Üzmez, Atmospheric ambient trace element concentrations of PM_{10} at urban and sub-urban sites: source apportionment and health risk estimation, *Environ. Monit. Assess.*, 2018, **190**, 1–17, DOI: 10.1007/s10661-018-6517-6.

64 L. S. P. Nguyen, T. T. L. Do, T. G. H. Vo, Q. H. Le and T. T. Hien, The source and distribution of heavy metals in

the atmosphere across Southeast Asia, in *Heavy Metal Remediation: Sustainable Nexus Approach*, Springer Nature Switzerland, Cham, 2024, pp. 1–26, DOI: 10.1007/978-3-031-53688-5_1.

65 B. Chen, A. F. Stein, P. G. Maldonado, A. M. S. de la Campa, Y. Gonzalez-Castanedo, N. Castell and J. D. de la Rosa, Size distribution and concentrations of heavy metals in atmospheric aerosols originating from industrial emissions as predicted by the HYSPLIT model, *Atmos. Environ.*, 2013, **71**, 234–244, DOI: 10.1016/j.atmosenv.2013.02.013.

66 Y. Dai, H. Dong, L. Sun, J. Li, T. Zhang, Y. Geng and Z. Liu, Life cycle environmental impact assessment of titanium dioxide production in China, *Environ. Impact Assess. Rev.*, 2024, **105**, 107412, DOI: 10.1016/j.eiar.2023.107412.

67 M. Keane, S. Stone, B. Chen, J. Slaven, D. Schwegler-Berry and J. Antonini, Hexavalent chromium content in stainless steel welding fumes is dependent on the welding process and shield gas type, *J. Environ. Monit.*, 2009, **11**(2), 418–424, DOI: 10.1039/B814063D.

68 B. de Foy, J. Heo, J. Y. Kang, H. Kim and J. J. Schauer, Source attribution of air pollution using a generalized additive model and particle trajectory clusters, *Sci. Total Environ.*, 2021, **780**, 146458, DOI: 10.1016/j.scitotenv.2021.146458.

69 X. Fu, M. Jiskra, X. Yang, N. Marusczak, M. Enrico, J. Chmeleff and J. E. Sonke, Mass-independent fractionation of even and odd mercury isotopes during atmospheric mercury redox reactions, *Environ. Sci. Technol.*, 2021, **55**(14), 10164–10174, DOI: 10.1021/acs.est.1c02568.

70 L. S. P. Nguyen and T. T. Hien, Long-range atmospheric mercury transport from across East Asia to a suburban coastal area in Southern Vietnam, *Bull. Environ. Contam. Toxicol.*, 2024, **112**(1), 14, DOI: 10.1007/s00128-023-03842-1.

71 S. Illuminati, A. Annibaldi, S. Bau, C. Scarchilli, V. Ciardini, P. Grigioni and C. Truzzi, Seasonal evolution of size-segregated particulate mercury in the atmospheric aerosol over Terra Nova Bay, Antarctica, *Molecules*, 2020, **25**(17), 3971, DOI: 10.3390/molecules25173971.

72 H. Zhou, C. Zhou, P. K. Hopke and T. M. Holsen, Mercury wet deposition and speciated mercury air concentrations at rural and urban sites across New York State: temporal patterns, sources and scavenging coefficients, *Sci. Total Environ.*, 2018, **637**, 943–953, DOI: 10.1016/j.scitotenv.2018.05.047.

73 Y. J. Han, J. E. Kim, P. R. Kim, W. J. Kim, S. M. Yi, Y. S. Seo and S. H. Kim, General trends of atmospheric mercury concentrations in urban and rural areas in Korea and characteristics of high-concentration events, *Atmos. Environ.*, 2014, **94**, 754–764, DOI: 10.1016/j.atmosenv.2014.06.002.

74 G. L. Simpson, Modelling palaeoecological time series using generalised additive models, *Front. Ecol. Evol.*, 2018, **6**, 149, DOI: 10.3389/fevo.2018.00149.

75 D. N. Asimakopoulos, T. Maggos and C. Vasilakos, Particulate matter levels in a suburban Mediterranean area: Analysis of a 53-month long experimental campaign, *J. Hazard. Mater.*, 2010, **182**, 801–811, DOI: 10.1016/j.jhazmat.2010.06.108.

76 C. Y. Hsu, K. H. Chi, C. D. Wu, S. L. Lin, W. C. Hsu, C. C. Tseng and Y. C. Chen, Integrated analysis of source-specific risks for $PM_{2.5}$-bound metals in urban, suburban, rural, and industrial areas, *Environ. Pollut.*, 2021, **275**, 116652, DOI: 10.1016/j.envpol.2021.116652.

77 P. Bertaccini, V. Dukic and R. Ignaccolo, Modeling the short-term effect of traffic and meteorology on air pollution in Turin with generalized additive models, *Adv. Meteorol.*, 2012, **2012**, 609328, DOI: 10.1155/2012/609328.

78 L. Yang, G. Qin, N. Zhao, C. Wang and G. Song, Using a generalized additive model with autoregressive terms to study the effects of daily temperature on mortality, *BMC Med. Res. Methodol.*, 2012, **12**(1), 165, DOI: 10.1186/1471-2288-12-165.

79 A. F. Zuur, E. N. Ieno and G. M. Smith, *Analysing Ecological Data*, Springer, New York, 2007, DOI: 10.1007/978-0-387-45972-1_12.

80 C. T. Driscoll, R. P. Mason, H. M. Chan, D. J. Jacob and N. Pirrone, Mercury as a global pollutant: sources, pathways, and effects, *Environ. Sci. Technol.*, 2013, **47**(10), 4967–4983, DOI: 10.1021/es305071v.

81 N. Pirrone, S. Cinnirella, X. Feng, R. B. Finkelman, H. R. Friedli, J. Leaner and K. Telmer, Global mercury emissions to the atmosphere from anthropogenic and natural sources, *Atmos. Chem. Phys.*, 2010, **10**(13), 5951–5964, DOI: 10.5194/acp-10-5951-2010.

82 U. Kurien, Z. Hu, H. Lee, A. P. Dastoor and P. A. Ariya, Radiation enhanced uptake of Hg^0(g) on iron (oxyhydr) oxide nanoparticles, *RSC Adv.*, 2017, **7**(71), 45010–45021, DOI: 10.1039/C7RA07401H.

83 E. Gaggero, M. J. López-Muñoz, M. C. Paganini, A. Arencibia, S. Bertinetti, N. Fernández de Paz and P. Calza, Mercury and organic pollutants removal from aqueous solutions by heterogeneous photocatalysis with ZnO-based materials, *Molecules*, 2023, **28**(6), 2650, DOI: 10.3390/molecules28062650.

84 F. Yue, H. Angot, H. Liu and Z. Xie, Marine phytoplankton and sea-ice initiated convection drive spatiotemporal differences in Arctic summertime mercury rebound, *Nat. Commun.*, 2025, **16**(1), 6075, DOI: 10.1038/s41467-025-61000-z.

85 Z. Xu, L. Chen, Y. Zhang, G. Han, Q. Chen, Z. Chu and X. Wang, Meteorological drivers of atmospheric mercury seasonality in the temperate Northern Hemisphere, *Geophys. Res. Lett.*, 2022, **49**(20), e2022GL100120, DOI: 10.1029/2022GL100120.

86 A. M. S. de la Campa, J. D. de la Rosa, J. C. Fernández-Caliani and Y. González-Castanedo, Impact of abandoned mine waste on atmospheric respirable particulate matter in the historic mining district of Rio Tinto (Iberian Pyrite Belt), *Environ. Res.*, 2011, **111**(8), 1018–1023, DOI: 10.1016/j.envres.2011.07.001.

87 S. Jain, S. K. Sharma, T. K. Mandal and M. Saxena, Source apportionment of PM_{10} in Delhi, India using PCA/APCS,

UNMIX and PMF, *Particuology*, 2018, **37**, 107–118, DOI: 10.1016/j.partic.2017.05.009.

88 W. Li, P. Ge, M. Chen, J. Tang, M. Cao, Y. Cui and D. Nie, Tracers from biomass burning emissions and identification of biomass burning, *Atmosphere*, 2021, **12**(11), 1401, DOI: 10.3390/atmos12111401.

89 H. Wen and J. Carignan, Reviews on atmospheric selenium: emissions, speciation and fate, *Atmos. Environ.*, 2007, **41**(34), 7151–7165, DOI: 10.1016/j.atmosenv.2007.07.035.

90 K. Guo, Y. Li, J. Wang, Z. Sui, T. Wang and W. P. Pan, A review on selenium in coal-fired power plants: content and forms in coal, determination methods, migration, transformation, and control technologies, *J. Environ. Chem. Eng.*, 2024, **12**(5), 113579, DOI: 10.1016/j.jece.2024.113579.

91 S. Ma, F. Xu, D. Qiu, S. Fan, R. Wang, Y. Li and X. Chen, The occurrence, transformation and control of selenium in coal-fired power plants: status quo and development, *J. Air Waste Manage. Assoc.*, 2022, **72**(2), 131–146, DOI: 10.1080/10962247.2021.2010620.

92 J. Yu, C. Yan, Y. Liu, X. Li, T. Zhou and M. Zheng, Potassium: a tracer for biomass burning in Beijing?, *Aerosol Air Qual. Res.*, 2018, **18**(9), 2447–2459, DOI: 10.4209/aaqr.2017.11.0536.

93 V. I. Babushok, P. Deglmann, R. Krämer and G. T. Linteris, Influence of antimony-halogen additives on flame propagation, *Combust. Sci. Technol.*, 2017, **189**, 290–311, DOI: 10.1080/00102202.2016.1208187.

94 J. Das, A. Kleiman, A. U. Rehman, R. Verma and M. H. Young, The cobalt supply chain and environmental life cycle impacts of lithium-ion battery energy storage systems, *Sustainability*, 2024, **16**(5), 1910, DOI: 10.3390/su16051910.

95 M. J. Pilat and R. C. Pegnam, Particle emissions from chrome plating, *Aerosol Sci. Technol.*, 2006, **40**(8), 639–648, DOI: 10.1080/02786820600763020.

96 W. H. Liao, S. Takano, H. A. Tian, H. Y. Chen, Y. Sohrin and T. Y. Ho, Zn elemental and isotopic features in sinking particles of the South China Sea: Implications for its sources and sinks, *Geochim. Cosmochim. Acta*, 2021, **314**, 68–84, DOI: 10.1016/j.gca.2021.09.013.

97 M. Pirhadi, A. Mousavi, S. Taghvaee, M. M. Shafer and C. Sioutas, Semi-volatile components of $PM_{2.5}$ in an urban environment: volatility profiles and associated oxidative potential, *Atmos. Environ.*, 2020, **223**, 117197, DOI: 10.1016/j.atmosenv.2019.117197.

98 L. Guan, Y. Liang, Y. Tian, Z. Yang, Y. Sun and Y. Feng, Quantitatively analyzing effects of meteorology and $PM_{2.5}$ sources on low visual distance, *Sci. Total Environ.*, 2019, **659**, 764–772, DOI: 10.1016/j.scitotenv.2018.12.431.

99 X. Feng, Y. Tian, D. Guo, Q. Xue, D. Song, F. Huang and Y. Feng, Quantifying role of source variations on $PM_{2.5}$-bound toxic components under climate change: measurement at multiple sites during 2018-2022 in a Chinese megacity, *J. Hazard. Mater.*, 2025, 138584, DOI: 10.1016/j.jhazmat.2025.138584.

100 I. Cheng, L. Zhang, P. Blanchard, J. Dalziel and R. Tordon, Concentration-weighted trajectory approach to identifying potential sources of speciated atmospheric mercury at an urban coastal site in Nova Scotia, Canada, *Atmos. Chem. Phys.*, 2013, **13**(12), 6031–6048, DOI: 10.5194/acp-13-6031-2013.